



ELSEVIER

Contents lists available at ScienceDirect

Continental Shelf Research

journal homepage: www.elsevier.com/locate/csr

Pathways and hydrography in the Mesoamerican Barrier Reef System Part 2: Water masses and thermohaline structure

L. Carrillo ^{a,*}, E.M. Johns ^b, R.H. Smith ^b, J.T. Lamkin ^c, J.L. Largier ^d^a El Colegio de la Frontera Sur, Departamento de Sistemática y Ecología Acuática, Av. Centenario km 5.5, Col. Pacto Obrero, 77014 Chetumal, Quintana Roo, Mexico^b NOAA Atlantic Oceanographic and Meteorological Laboratory, 4301 Rickenbacker Causeway, Miami, FL 33149, USA^c NOAA National Marine Fisheries Service, Southeast Fisheries Science Center, 75 Virginia Beach Drive, Miami, FL 33149, USA^d Bodega Marine Laboratory, University of California Davis, PO Box 247, Bodega Bay, CA 94923, USA

ARTICLE INFO

Article history:

Received 12 May 2015

Received in revised form

24 February 2016

Accepted 5 March 2016

Available online 16 March 2016

Key points:

Description of water masses in the Mesoamerican Barrier Reef System, with local influences due to upwelling and land runoff.

Index terms:

4220 (Coral reef systems)

4223 (Descriptive and regional oceanography)

4512 (Currents)

4520 (Eddies and mesoscale processes)

Keywords:

Yucatan Current

Mesoamerican Barrier Reef

Hydrography

Water masses

Geostrophy

ABSTRACT

Hydrographic data from two oceanographic cruises conducted during March 2006 and January/February 2007 are used to investigate the thermohaline structure related to the observed circulation along the Mesoamerican Barrier Reef System (MBRS). From our observations we identify three water masses in the MBRS: the Caribbean Surface Water (CSW), North Atlantic Subtropical Underwater (SUW), and Tropical Atlantic Central Water (TACW). Little vertical structure in temperature is observed in the upper 100 m of the water column, but important differences are observed in the salinity distribution both horizontally and with depth. Freshwater inputs to the system from the mainland can be traced in the surface layer, with two possible sources: one from surface rivers located along the southern portion of the MBRS, and the other originating from an underground river system located along the northern portion of the MBRS. The thermohaline structure in the MBRS reflects the dynamics of the observed circulation. Uplifted isopycnals along most of the central and northern coastline of the MBRS reflect the effects of the strong geostrophic circulation flowing northward, i.e. the Yucatan Current. To the south along the MBRS, much weaker velocities are observed, with the Honduras Gyre dominating the flow in this region as presented during January/February 2007. These two regions are separated by onshore and divergent alongshore flow associated with the impingement of the Cayman Current on the shore and the MBRS.

© 2016 Elsevier Ltd. All rights reserved.

1. Introduction

Our knowledge of the hydrographic and water mass characteristics of the Mesoamerican Barrier Reef System (MBRS) relies primarily on studies from nearby regions such as the Gulf of Mexico, the Lesser Antilles, the Windward Passage, the Straits of Florida, the coast of Venezuela, and the Yucatan Channel area (c.f. Wüst, 1964; Lambert and Sturges, 1977; Morrison and Nowlin, 1982; Tomczak and Godfrey, 2003; Hernandez-Guerra and Joyce, 2000). In general, the MBRS receives water masses that are imported by the Caribbean Current, having entered from the Atlantic Ocean through the multiple passages between the northern and eastern Caribbean islands. En route to the MBRS the water masses

are modified by mixing with ambient water masses, air-sea exchange (evaporation, precipitation, heating, cooling), and freshening by land runoff. In addition, extreme weather events occur at times, capable of producing dramatic changes in the thermohaline structure of the water masses (Jaimes and Shay, 2009). Finally, once the water masses arrive at the MBRS, the spatial distribution of thermohaline properties is determined by the circulation, which is dominated by the strong, northward-flowing Yucatan Current in the northern MBRS, the presence of weaker southward currents and the mesoscale Honduras Gyre in the southern MBRS, and the impingement of the Cayman Current onto the coast, which forms a hydrographic boundary between the northern and southern regions (Carrillo et al., 2015).

How hydrographic structures and their variability in the MBRS are related to the regional circulation is poorly understood. Most physical oceanographic studies in the MBRS and the greater western Caribbean have concentrated on basin-scale circulation,

DOI of original article: <http://dx.doi.org/10.1016/j.csr.2015.09.014>

* Corresponding author.

E-mail addresses: lcarrillo@ecosur.mx, laucarrillo@gmail.com (L. Carrillo).

leaving regional hydrographic characteristics unexplored. This is particularly true for how the water masses and thermohaline structure relate to the circulation. Thus, there is a critical need for regional hydrographic observations using traditional shipboard oceanographic methods that have not often been employed in the MBRS during the last two decades.

The need for regional oceanographic study of the MBRS is made urgent by the recent report of the Status and Trends of Caribbean Coral Reefs 1970–2012 (Jackson et al., 2014), in which it is reported that coral coverage in the MBRS is in a dramatic decline, and that the reefs may even disappear in this region in the next 20 years. This is an alarming prognosis for the MBRS, the second largest barrier reef in the world and the largest in the Atlantic Ocean. It is well known that one of the primary factors affecting coral reef growth is the water quality of the surrounding water column (Nichols and Williams, 2009), yet the thermohaline structure and chemical properties of the waters over the MBRS remain poorly

known, and a baseline does not yet exist for this region. Beyond direct influences on coral physiology, both the hydrographic conditions and the regional circulation influence the dynamics of benthic and pelagic communities that interact with the reef ecosystem (Nichols and Williams, 2009) and the circulation is a primary factor in connectivity along the MBRS. The lack of physical oceanographic observations in the MBRS is in sharp contrast to the urgent need to understand the future of this biodiverse and yet fragile ecosystem.

Here we report on two recent surveys and present new information on the water masses and hydrography along the MBRS. What water masses are present along the MBRS? How does the regional circulation explain the distribution of these water masses and associated hydrographic structure? How do local processes modify water mass characteristics and associated horizontal and vertical distributions of temperature and salinity? The aim of this work is to provide a regional baseline of the thermohaline

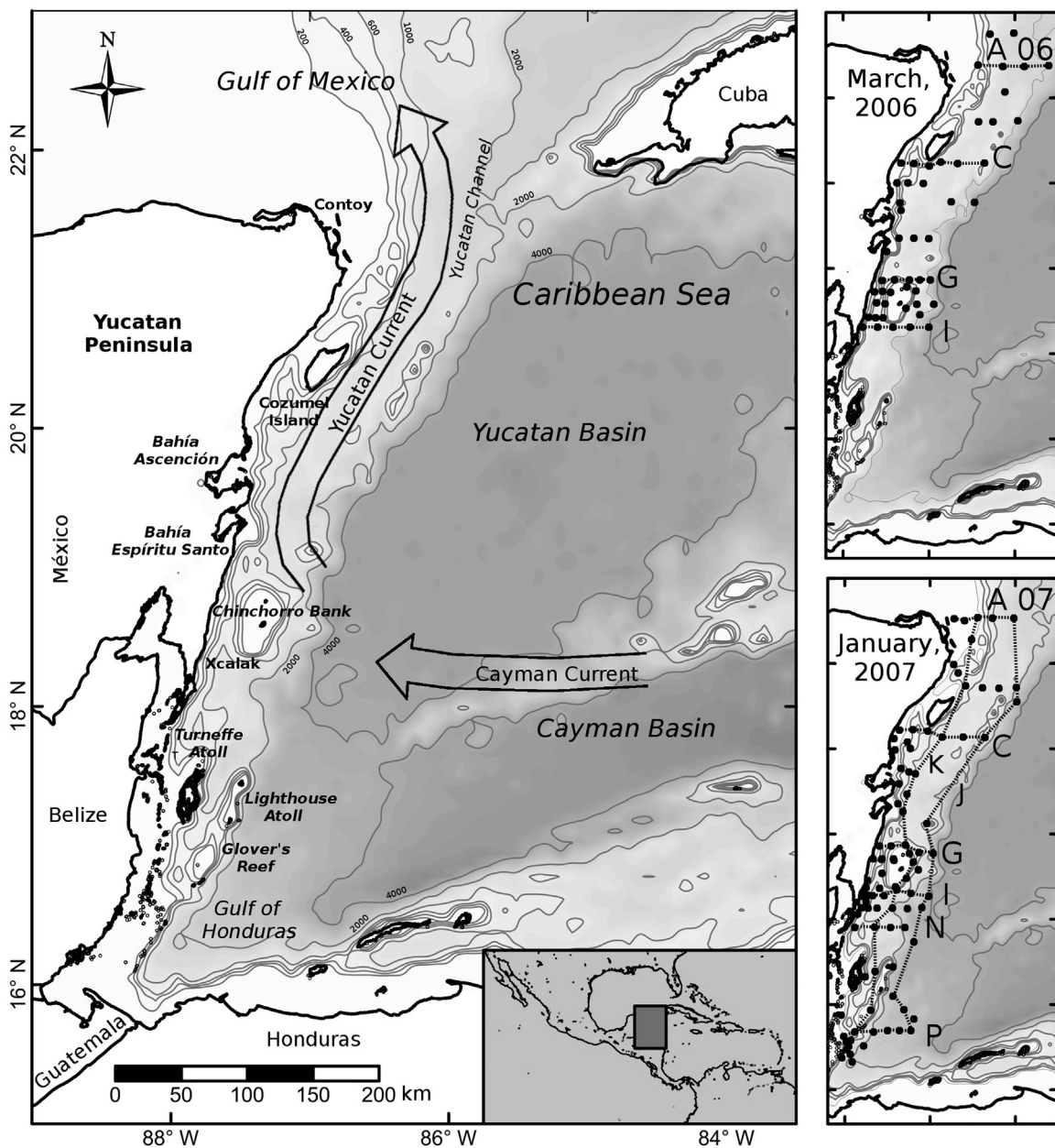


Fig. 1. a) Study area showing Western Caribbean Sea basins, the narrow shelf and other selected bathymetric features offshore of the Mesoamerican Barrier Reef region. Bathymetry is shaded in gray, with thick contours at 1000, 2000, 3000, and 4000 m, and shows the narrow shelf. Selected cross-sections (dashed lines) and hydrographic stations for b) March 2006 and c) January 2007 are also shown.

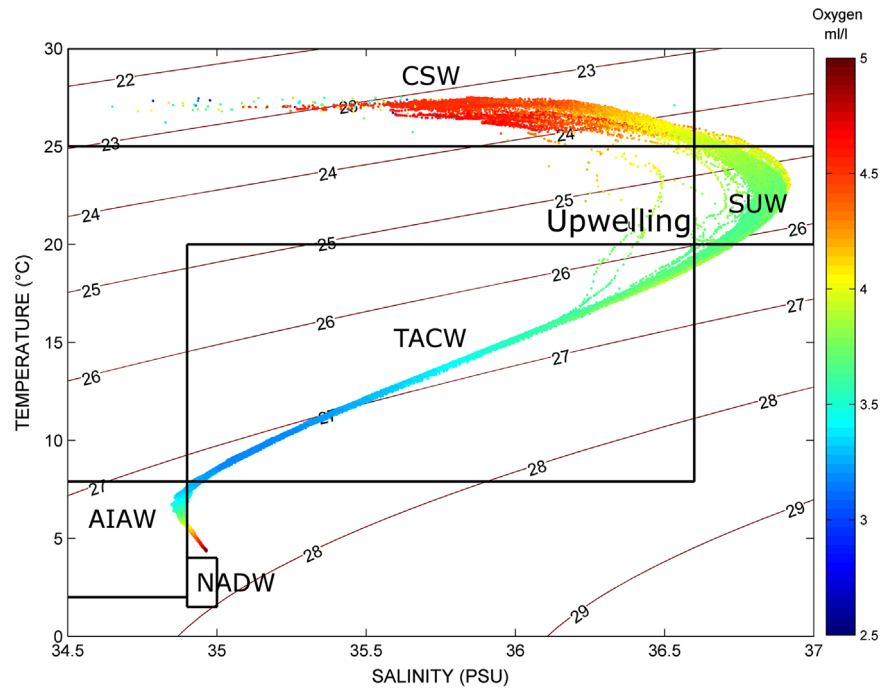


Fig. 2. Temperature-Salinity diagram with water masses delimited by squares according to the ranges of values listed in Table 1. Color indicates oxygen content. Values outside the mean curve are labeled as “Upwelling” and correspond to casts from the area near Contoy Island. (For interpretation of the references to color in this figure legend, the reader is referred to the web version of this article.)

structure and water masses of the MBRS and their interaction with the observed circulation. This information will guide regional resource management and also be valuable for validation of numerical models.

In order to achieve these goals, a set of conductivity-temperature-depth (CTD) data from two oceanographic surveys conducted during March 2006 and January/February 2007 was used. We focus herein on the upper water masses (above 500 m depth), where a relatively rapid rate of renewal, transport, and distribution depends strongly on the regional circulation. This is the second part (Part 2) of the Pathways and Hydrography in the Mesoamerican Barrier Reef System study, providing the first detailed examination of water masses and the thermohaline structure along the MBRS and its relationship with the circulation as observed and reported in Part 1 (Carrillo et al., 2015).

2. Data and methods

Hydrographic data were collected in the MBRS during two oceanographic cruises conducted aboard the NOAA Ship *Gordon Gunter* during March 2006 and January/February 2007 (hereafter M06 and J07). The station array was selected to provide a measure of larval fish diversity and abundance while also resolving the major oceanographic features, involving a trade-off between density of stations and spatial coverage (Fig. 1). At each station, CTD casts were obtained using a Sea-Bird Electronics (SBE) Model 911 Plus system configured with dual temperature (SBE 3), conductivity (SBE 4), and oxygen sensors (SBE 43), chlorophyll *a* (chl_a) fluorometers (WET Labs ECO FL), and a 24-Niskin bottle water sampler. Post-cruise processing of the CTD data set was performed using standard techniques. Most CTD casts were taken from the surface to 500 m depth, although some deeper casts were also obtained. During M06, the Mexican Caribbean (extending from the Yucatan Channel to the border between Mexico and Belize) was surveyed with a total of 51 CTD casts. During J07, the Belizean, Guatemalan and Mexican coasts were surveyed with a

total of 95 CTD stations.

Geostrophic velocity fields were obtained from dynamic height differences derived from the density anomaly fields, assuming a level of no motion along the isopycnal $\sigma_t = 27.0 \text{ kg m}^{-3}$. We chose this σ_t isopycnal as the no-motion reference level after comparing Acoustic Doppler Current Profiler (ADCP) data (Carrillo et al., 2015) with geostrophic velocity fields derived by using different water depths (e.g., 500 m) and σ_t isopycnals for the no-motion reference level. While geostrophic velocities were very similar to ADCP velocities in general (not shown), at specific stations geostrophic estimates underestimated ADCP-observed magnitudes by ± 0.05 – 0.15 m/s, but up to 0.5 m/s on the northernmost sections. The geostrophic field was derived from vertical integration of the thermal-wind equation above the depth of the isopycnal $\sigma_t = 27.0 \text{ kg m}^{-3}$. Objective mapping was used to obtain smoothed gridded fields according to Carrillo et al. (2002).

To describe the thermohaline structure along the MBRS, we selected the following cross-sections: Line A, the northernmost section offshore Contoy Island to ~ 115 km offshore; Line C, located 60 km north of Bahía de la Ascension and south of Cozumel Island; Lines G and I, north and south of Chinchorro Bank, respectively, and in the Cayman Current impingement zone; and Lines N and P, which are representative cross-sections in Belizean coastal waters, with Line P just south of Glovers Reef and in the Gulf of Honduras. Lines N and P were only occupied during 2007. Since the location of Line A was different in the M06 and M07 cruises, it is labeled as Line A06 and Line A07, respectively.

3. Results

3.1. Water masses

A temperature-salinity diagram for all data shows the water masses present during the M06 and J07 cruises (Fig. 2) – and associated oxygen concentrations. The water masses are delineated by lines in Fig. 2, and the definitions of the water masses are listed

Table 1

Water mass definitions for the MBRS, range of values obtained from our shipboard data, and the water mass properties defined by Gallegos (1996).

	ID	Temp (°C)	Sal (psu)	Density (kg/m ³)	Depth (m)	Observations
Caribbean Surface Water	CSW	≥ 25	34.5–36.6	< 24.52	0–100	Surface Warmer Layer, Mixed Layer
North Atlantic Subtropical Underwater	SUW	19.0–26	36.6–37	24.24–26.25	50–250	Maximum salinity, Sal ≥ 37, 25.4 kg/m ³ centered at approx 150 m, Subtropical origin
Tropical Atlantic Central Water	TACW	7.9–20	34.9–36.6	26.25–27.2	300–600	Low oxygen, tropical Atlantic origin
Antarctic Intermediate Water	AAIW	2.0–7.9	33.8–34.9	27.2–27.47	600–900	Low salinity signal
North Atlantic Deep Water	NADW	1.5–6.0	34.9–35.0	> 27.47	900–bottom	Labrador sea origin

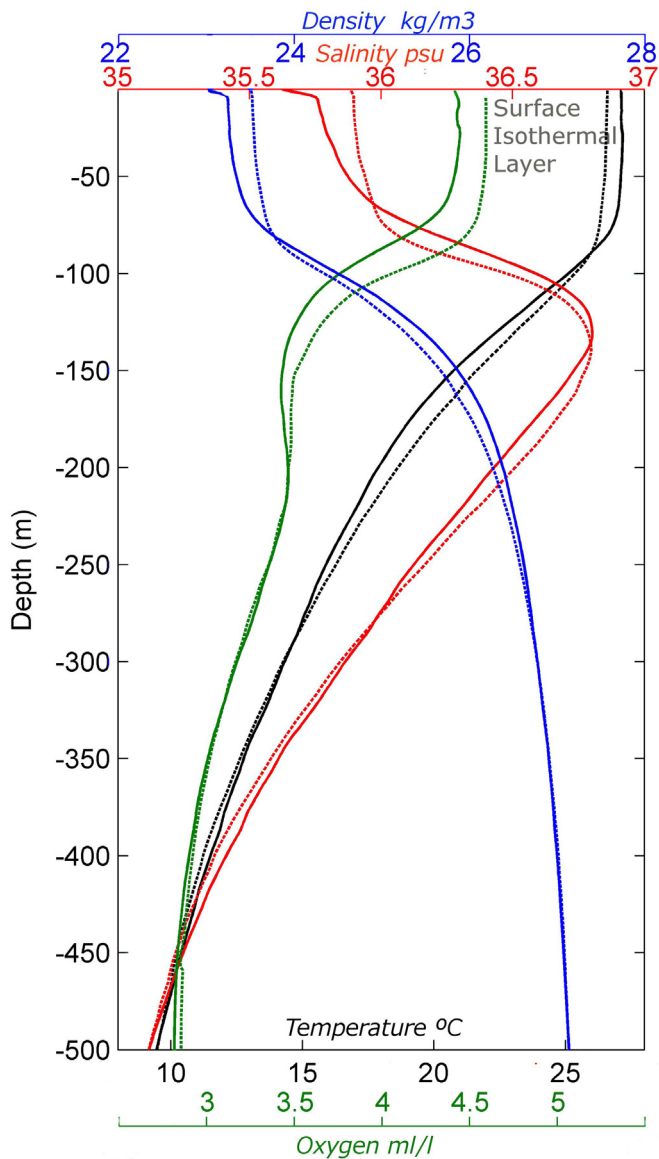


Fig. 3. Mean vertical profiles of temperature (black: °C), dissolved oxygen (green: ml/L), salinity (red), and density (blue: kg/m³) for the uppermost 500 m. M06 profiles are shown as dashed lines, and J07 profiles as solid lines. (For interpretation of the references to color in this figure legend, the reader is referred to the web version of this article.)

in Table 1. In order to maintain consistency with water mass names for the North Atlantic and Caribbean Waters, we use water mass definitions from Gallegos (1996). However, we extend the definitions of the water masses for this region because the salinity and temperature ranges differed from those that have been defined for regions closer to the entrance to the Caribbean Basin and

those summarized by Gallegos (1996) and Gallegos and Czitrom (1997). The five primary water masses of the Caribbean basin were present off the MBRS during our cruises:

- Caribbean Surface Water (CSW) – 4% of the volume of the Caribbean.
- North Atlantic Subtropical Underwater (SUW) – 5% of the volume of the Caribbean; formed in central tropical Atlantic.
- Tropical Atlantic Central Water (TACW) – 12% of the volume of the Caribbean; mixture of North and South Atlantic Central Waters.
- Antarctic Intermediate Water (AAIW) – 6% of the volume of the Caribbean; formed at the Sub-Antarctic Front.
- North Atlantic Deep Water (NADW) – 73% of the volume of the Caribbean.

The well-mixed warm surface layer off the MBRS is comprised of CSW, with salinity modified by local precipitation, runoff, and upwelling (Wüst, 1964; Hernandez-Guerra and Joyce, 2000). Dissolved oxygen is ≥ 4 ml/L with maximum values up to 4.67 ml/L. The high-salinity SUW lies beneath the CSW. Centered at about 150 m depth, the SUW is represented in our data with a maximum salinity of 36.92 in its core and a dissolved oxygen content of 3.37–4.06 ml/L. Merino (1997) referred to this water mass as Subtropical Intermediate Water (STUW 23 °C and 36.89 salinity) and Enriquez et al. (2013) named Caribbean Subtropical Underwater (CSUW) in the Yucatan Shelf with temperature values of 22–26 °C and salinity values of 36.4–36.7. From about 200 m to below 500 m the TACW is found, with oxygen decreasing to as low as 2.82 ml/L at depth. The TACW exhibits a tighter range of values, indicating less modification through mixing, and surface/land influences. Below the TACW one finds the low-salinity AAIW with salinities about 34.9 and oxygen about 3.5 ml/L. Finally, the deepest areas (> 950 m) are filled with NADW, cold waters with high levels of oxygen, up to ~5 ml/L. In this work, we address only waters above 500 m depth, which excludes the Intermediate and Deep water masses.

Mixing and water mass modification are evident in Fig. 2. The CSW water mass is being formed by the addition of freshwater combined with heating near the surface. The lowest CSW salinity values were observed at locations close to freshwater sources along the MBRS. Also, mixing is evident between the uppermost part of the TACW and CSW, yielding waters that are of the same density as SUW but markedly fresher (Fig. 2: these points deviate from the main temperature-salinity curve at temperatures between 16 and 26 °C). These data correspond to CTD casts taken near Contoy Island in the north and close to the Yucatan coast (Fig. 1), a region characterized by upwelling (Cochrane, 1966, 1968, 1969; Ruiz, 1979; Merino, 1997). We refer to this upwelled water again below.

3.2. Vertical profiles

Mean vertical profiles of temperature, salinity, density and

dissolved oxygen are shown in Fig. 3. The surface mixed layer was defined by the depth at which the temperature is 0.8 °C cooler than the surface (c.f., threshold approach used by Kara et al. (2003)). This surface layer has a mean thickness of 93 m and a mean temperature of 26.5 °C during M06 (dashed lines), and 85 m and 27.12 °C during J07 (solid lines). Below this layer, temperature decreases monotonically (~ -0.062 °C/m) towards the 200 m depth. From 200 m to 500 m depth it decreases at a rate of -0.025 °C/m.

Salinity is lowest in the surface layer, with markedly lower values in the uppermost 5–10 m (lowest during J07). Maximum salinity is observed in the SUW between 110 and 150 m with peak values at 135 m and 124 m in M06 and J07, respectively. Below this maximum, salinity decreases monotonically (~ -0.005 /m) to 500 m depth.

Density profiles exhibit a surface mixed layer with a well-defined pycnocline, below which stratification decreases slowly with depth. Surface densities are very low due to the combination of high temperature and low salinity values (CSW), and density increases rapidly over 50 m with the transition to the colder, high-salinity SUW. Locally the stratification can attain values of ~ 0.05 kg/m⁴, representing high stability. The depth of the pycnocline does not coincide exactly with that of the thermocline; it is shallower due to the influence of salinity. The barrier layer thickness, defined as the depth difference between the thermocline and the pycnocline (de Boyer Montégut et al., 2007), was 14 m during M06 and 17 m during J07.

The vertical profile of dissolved oxygen shows two local minima. The shallower minimum (~ 3.4 ml/L) is found in the core of the salinity maximum layer (SUW), and the deeper oxygen minimum (~ 2.8 ml/L) is found in the lower TACW near 500 m. Surface waters contain the most oxygen (4.7 and 4.4 ml/L for M06 and J07, respectively).

Salinity is most variable above the pycnocline (Fig. 4), and also below the core of the SUW where mixing with TACW is observed. In the top 40 m of the water column, salinity can be as low as 34.5 or as high as 36.1 (Fig. 2). Between 40 and 80 m depth, the salinity values are > 35.85 but < 36.8 . Below 100 m depth, the salinity is > 36.0 and increases until a maximum salinity is observed between 120 and 140 m, which represents the core of the SUW. The halocline can be as shallow as 5 m or as deep as 130 m, with a tradeoff between depth and intensity (Fig. 4): where freshwater inputs are retained near-surface, shallow haloclines are observed

with $\Delta S > 1.0$ whereas where freshwater is mixed to depth, haloclines are deeper and weaker with $\Delta S \leq 0.5$.

3.3. Hydrographic sections

Vertical structure changes with distance from the coast, due to upwelling and runoff effects. This is evident in the hydrographic sections plotted in Figs. 5–10.

The northernmost section (Lines A06, A07, Fig. 5) is characterized by an upward displacement of the water masses close to the shelf in both cruises. At the shelf edge the 25 °C isotherm is displaced 100 m and the 21 °C isotherm is displaced 150 m above their offshore depths. Maximum salinity of 36.85 is centered between 100 and 200 m depth (shallower nearer to the shelf). In J07 this SUW is observed at depths of 20–30 m over the shelf adjacent to Contoy Island, with salinity lowered by mixing with both SUW and CSW, which are also found over the shelf in this upwelling region. Local freshwater runoff is also evident in a thin layer with $S < 35.5$.

In the section located immediately south of Cozumel (Line C, Fig. 6), the uplifting of the water masses is less evident near-surface but uplifting of the TACW by 100 m or more was observed at depth. Salinity in the uppermost 50 m depth was patchy, due to local influences. During M06, a low-salinity layer was found offshore, with values ≤ 35.75 down to 40 m, and in J07 a shallower layer with surface salinity < 35.25 was observed. Following the isoline that separates CWS from SUW, a dome centered at ~ 35 –40 km can be observed during both M06 and J07. The vertical structure of SUW in this area resembles a lens typical of an eddy-like feature.

In sections along Lines G and I, north and south of Chinchorro Bank, there are notable differences between M06 and J07 (Figs. 7 and 8). In general, the upward displacement of the isotherms near the coast is much weaker than it was for the northern lines (A and C). While uplifting > 100 m is evident at depth during J07, uplifting is < 50 m in M06 on Line G (Fig. 7). In M06, isolines closer to the surface are not uplifted – in fact the isohalines above SUW deepen towards the coast on both lines G and I, indicating southward flow (based on geostrophy). Near the surface, a thin low-salinity layer is evident nearshore in both years and on both lines, with surface values being as low as 34.0 on Line G in J07 – presumably indicating local sources.

Belizean waters at the southernmost extent of the MBRS were only sampled during J07 (Lines N and P; Figs. 9 and 10). There is a marked low-salinity surface layer in this region, only 10 m deep on Line N and mixing down to 30 m on Line P. Salinities are lower and the largest area of freshwater influence was observed along these southern lines. A slight uplifting of the isolines is observed at Line N (Fig. 9) and a slight downward bending of isolines is observed in the southernmost transect, Line P (Fig. 10).

3.4. Horizontal thermal structure

The depth of the surface mixed layer is mapped for M06 and J07 in Fig. 11. The depth of this thermal layer is greater offshore than in the coastal waters. On the northernmost lines close to the Yucatan shelf, this layer is ~ 50 m thick during both cruises. Elsewhere along the coast, the surface mixed layer extends to 80–90 m whereas depths of 120 m are found offshore during M06 and 100 m offshore during J07. The temperature field at 150 m depth shows colder water close to the coast (Fig. 11c and d), with lower values during J07 than M06 in the area between Cozumel and Chinchorro. At the northern limit of the cruise, the coldest waters were observed in M06: the minimum 150 m temperature is 16 °C (2 °C lower than J07) and shows a strong thermal gradient of 6 °C/37 km along the offshore edge of the cold water. However, during

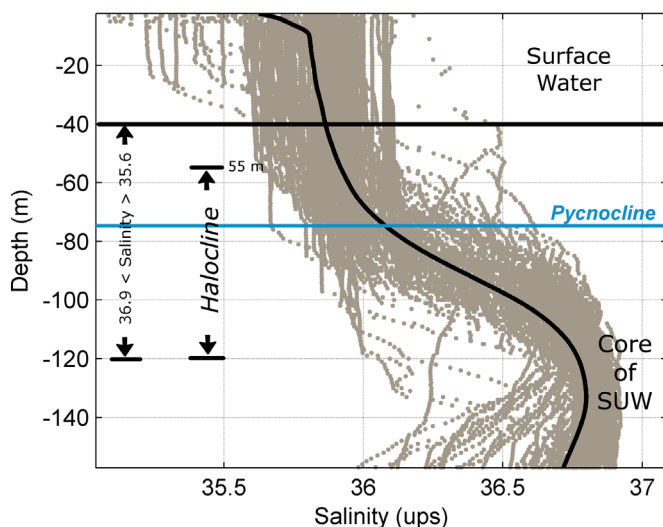


Fig. 4. Vertical profiles of salinity for the uppermost 150 m, showing the nearly homogeneous surface water, near-surface halocline, and the core of the SUW. The thick line shows the mean salinity profile over both cruises.

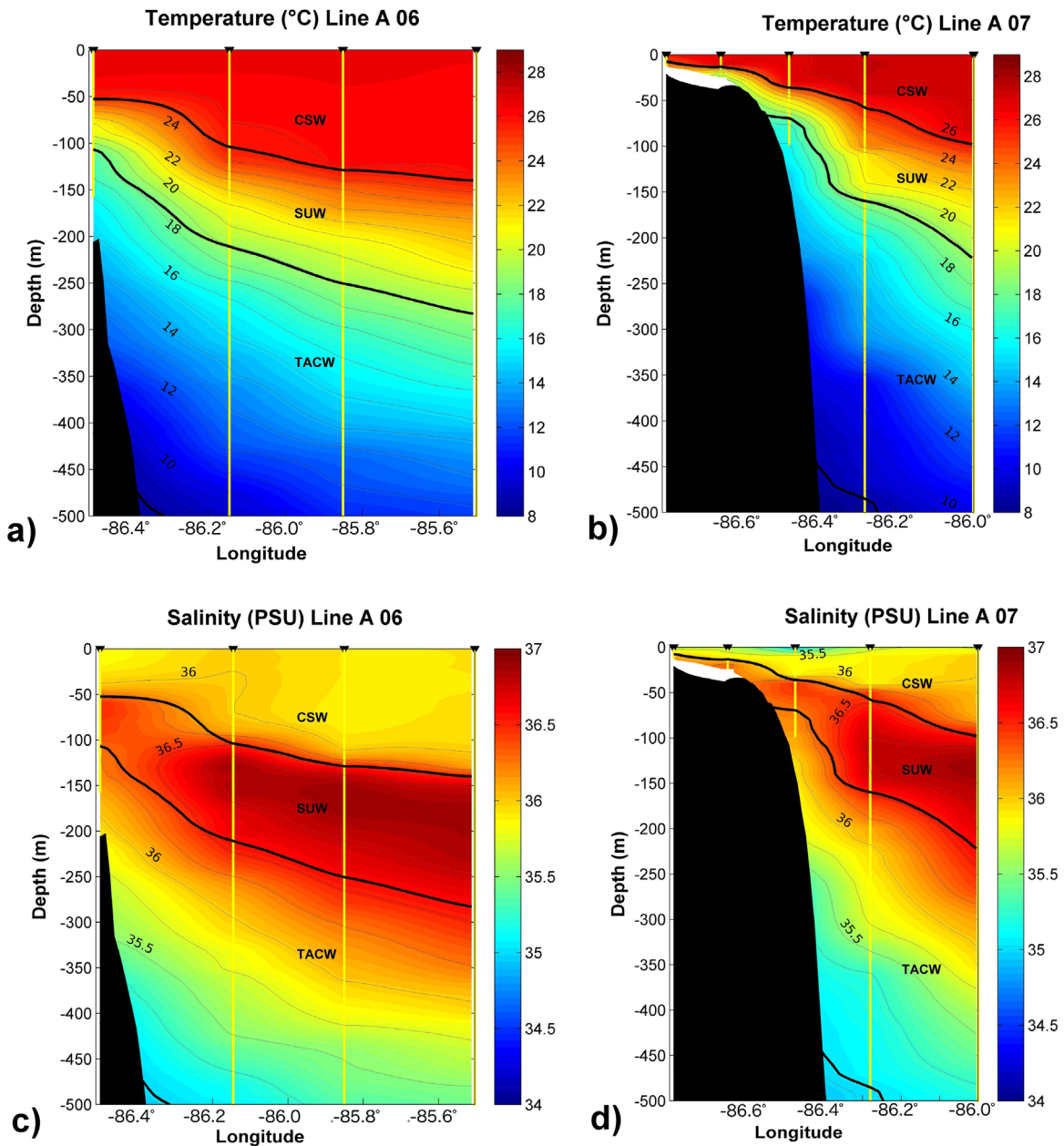


Fig. 5. Cross-sectional distribution of temperature and salinity at the northernmost section of the MBRS (Lines A06 and A07) between the surface and 500 m. Contours for salinity are in increments of 0.25, temperature contours in increments of 1 °C. The thick black lines delineate the water masses. The stations are marked at the top. a) Temperature, M06; b) Temperature, J07; c) Salinity, M06; and d) Salinity, J07.

J07, the 20 °C isotherm is observed as far south as Xcalak (~18.5°N). The same isotherm is only evident in the northern portion of the MBRS, north of Bahía de la Ascension (~20.0°N) in M06. During J07 a relatively strong thermal gradient was observed at 150 m between the coast and offshore waters (4 °C/37 km) in the area between the southern end of Cozumel and northern Chinchorro Bank, while it is weaker during M06 in the same area.

The horizontal distributions of the 12 and 22 °C isotherms are shown in Fig. 12. The 12 °C topography (Fig. 12a and b) gives an indication of the uplifting of the isotherms located at the lower base of the upper water masses, and the topography of the 22 °C isotherm (Fig. 12c and d) is used to illustrate the upward displacement of the isotherms, similarly to the way in which Merino (1997) used the 22.5 °C isotherm to demonstrate upwelling over the Yucatan shelf. In addition, the 22 °C isotherm is relatively close to 20 °C, which is considered the upper limit of the permanent thermocline in the tropics (Tomczak and Godfrey, 2003). The

topographies of both the 12 °C and 22 °C isotherms show an uplifting close to the coast during both cruises. Depth differences of the 12 °C isotherm between offshore and onshore waters are up to 200 m and 250 m during M06 and J07, respectively. During J07, the 12 °C isotherm is shallower close to the coast and considerably shallower close to the Yucatan shelf, with values up to 250 m, whereas just north of Bahía de la Ascension it is about 200 m depth. During J07, the 12 °C isotherm in the Belizean and Gulf of Honduras waters shows depths ~350–400 m, deeper than those observed in the Mexican Caribbean coastal waters. Differences between both cruises are found around Chinchorro Bank, where the 12 °C isotherm is relatively shallower during M06 than during J07.

Both cruises show an uplifting of the 22 °C isotherm from deep waters towards the coast. This isotherm is observed at depths > 170 m in oceanic waters, whereas it is observed at about 130 m in coastal waters. As was observed in other thermal topographies,

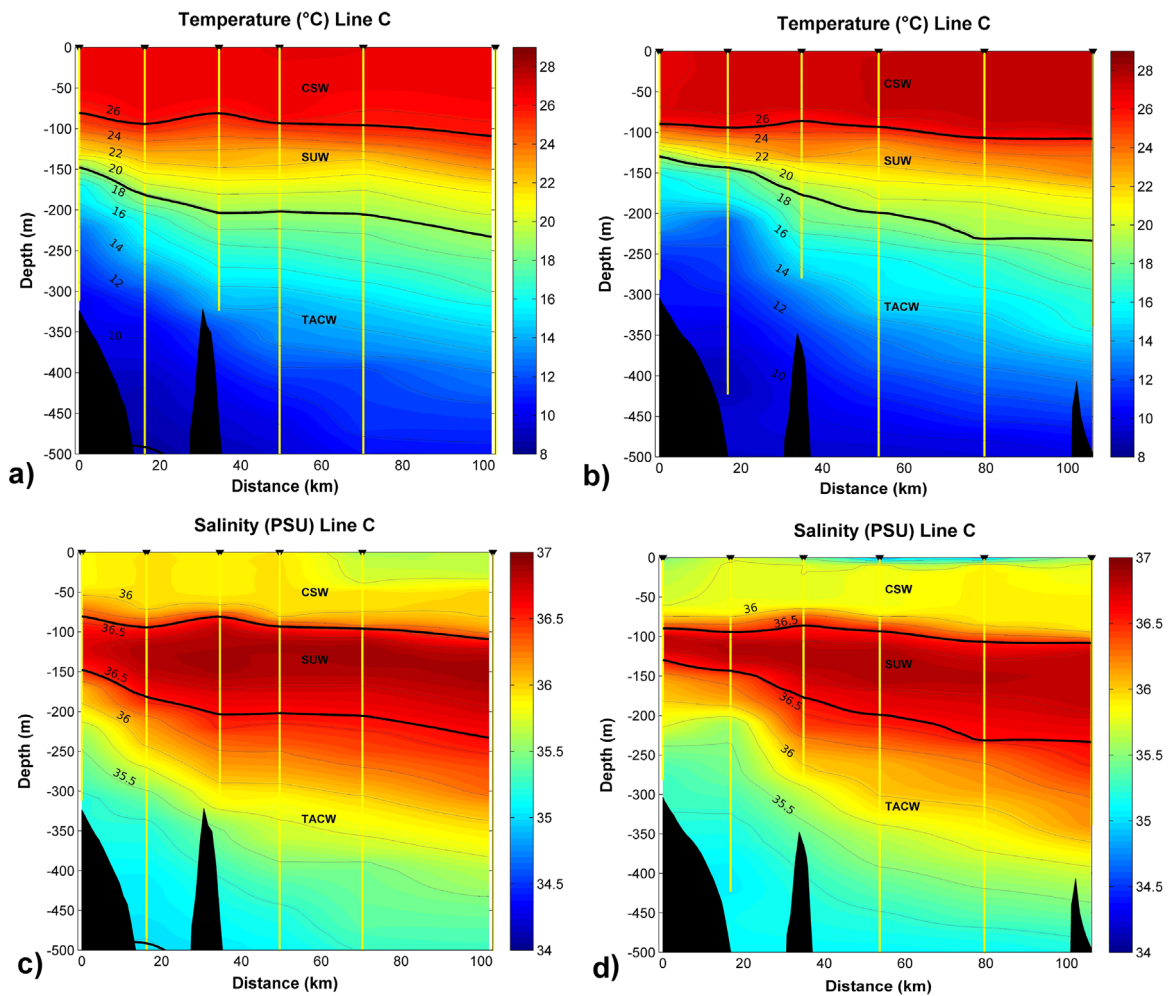


Fig. 6. Same as Fig. 5, but for the cross-section south of Cozumel Channel (Line C).

there are some coastal areas with considerable uplifting. The rising of the isotherm can be traced as far south as Xcalak (about 18.25°N), and it intensifies northwards along the coast, with a maximum on the Yucatan shelf. This isotherm is close to the surface in the northern MBRS near the Yucatan shelf, where it reaches depths as shallow as 20 m and 80 m during J07 and M06, respectively. Another shallow area was seen between the south end of Cozumel Island and latitude of about 19.25°N (around the bays of Ascension and Espiritu Santo), where it is observed at 120 m and up to 110 m near Bahía Ascension during J07.

3.5. Horizontal salinity structure

There is high variability of the surface salinity data within the first 120 m (Fig. 4). Horizontal salinity distribution maps at 5 m, 25 m (near the surface, below the halocline), 50 m (top of the halocline) and 75 m (within the halocline) were selected for the analysis. In general, during both cruises, the surface salinity shows patchiness and lower salinity near the coast.

During M06, over a large portion of the sampled area of the MBRS, the 5 m salinity is ≤ 35.8 (Fig. 13a). As the salinity increases with depth some patterns emerge, such as near the northern tip of the MBRS where uplifted high-salinity waters representing the SUW are observed in the 50-m and 75-m salinity distributions (Fig. 13c and d). Also, with increasing depth, it becomes evident that there is relatively saltier water there than is found in the coastal waters over Chinchorro Bank. A large lens of lower salinity water, at about 50 m depth, is observed close to the Yucatan Basin

(southeast of Cozumel Island).

During J07, the whole coast of the MBRS shows 5 m salinities lower than 35.8 (Fig. 13e), as also seen during M06, with two relatively large areas showing particularly low salinities (as low as 35.2). One is located in the northern MBRS (from Espiritu Santo and Bahía de la Ascension to Isla Contoy), and the second is located in the southern MBRS (near Belize/Gulf of Honduras). The northern low-salinity area is present at both 25 m and 50 m depth (Fig. 13g), and the salinity anomaly is reduced to a small portion of low-salinity water (35.8) at 75 m depth (Fig. 13h) located near the coast north of Bahía de la Ascension. The southern low-salinity area, located in the Gulf of Honduras, can be traced at 25 m depth (Fig. 13f), but is weak at 50 m (Fig. 13g) and not clear by 75 m (Fig. 13h). As was observed for M06, the central MBRS area around Chinchorro Bank (18–19°N) shows relatively higher salinity values at the surface during J07, and at 25 and 50 m depth. Higher salinity values were also observed in the northernmost part of the MBRS at 50 m depth, generating strong salinity gradients of about 0.4/48 km. At 75 m depth, except in the northern MBRS, the whole area shows salinity values greater than 36.0, in contrast to those of the salinity field at 50 m. In particular, in the Gulf of Honduras and north of Cozumel the salinity field shows higher values (> 36.4). Although most of the coast shows relatively high salinity values at this depth, one station at about 20 km from the coast north of Bahía de la Ascension shows lower salinity values (35.9).

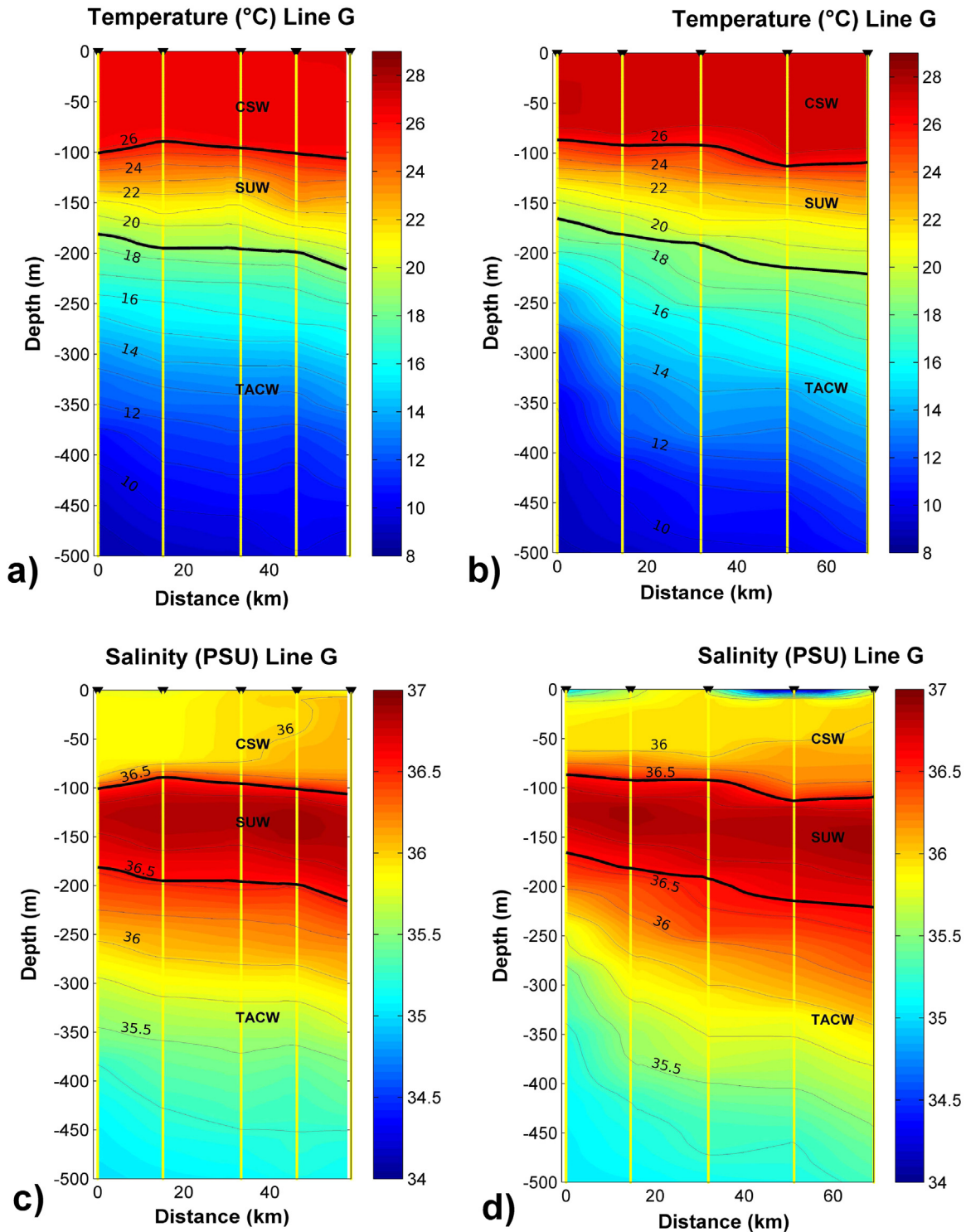


Fig. 7. Same as Fig. 5, but for the cross-section north of Chinchorro Bank (Line G).

3.6. Geostrophic velocity fields

Geostrophic velocities from the M06 and J07 cruises were calculated from dynamic height differences derived from the density anomaly fields (Fig. 14a and b). The isopycnal $\sigma_t = 27.0 \text{ kg m}^{-3}$ was used as the level of no motion. Geostrophic flow fields were improved by combining altimetry-derived flows and geostrophic velocities derived from hydrography. The altimetry-derived geostrophic currents were obtained from the Rio05 output model estimated from dynamic topography averaged over

a 10-day period (Rio and Hernandez, 2004). The time periods used in this analysis correspond to March 26–30, 2006 and January 17–22, 2007 for M06 and J07, respectively. Both cruises show similar surface geostrophic velocity fields, with strong northward flow of the Yucatan Current in the northern portion of the MBRS and relatively weaker velocities in the southern portion. During M06 (Fig. 14a), the Chinchorro area shows weak flows, indeed southward flows were obtained at the southern portion of this bank. The northward flow of the Yucatan Current is best defined between a latitude of approximately 19.25°N up to the Yucatan

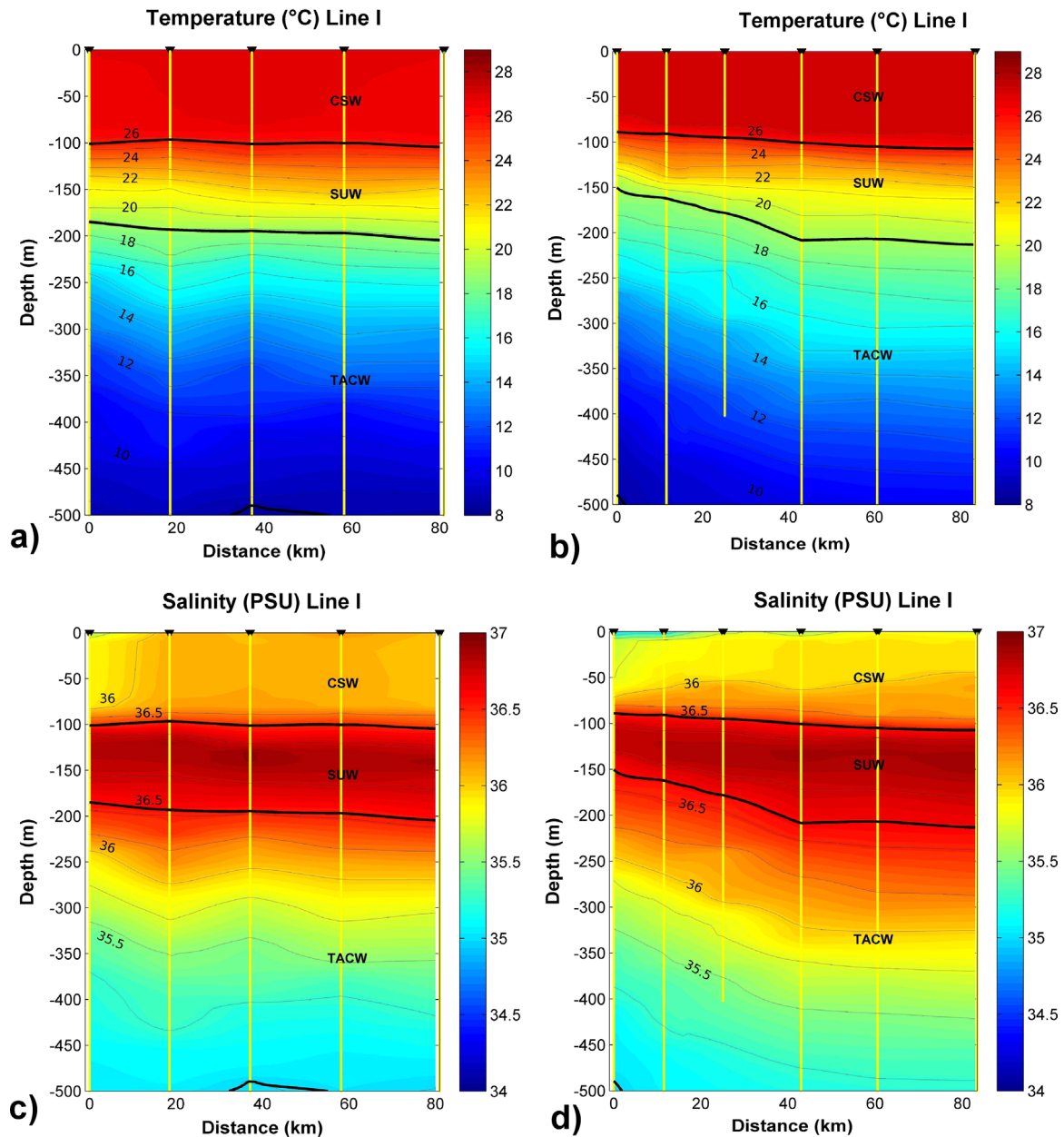


Fig. 8. Same as Fig. 5, but for the cross-section south of Chinchorro Bank (Line I).

Channel. During J07 (Fig. 14b), northward geostrophic velocities are clearly defined from 18.25°N to farther north, and were closer to the coast and confined in a narrower area than had been observed during M06 (Fig. 14a). In the Gulf of Honduras, the geostrophic field showed the weakest velocities and a southward flow (Fig. 14b).

Cross-sections of geostrophic velocity were estimated for the previously described hydrographic lines by using the level of no motion of $\sigma_t = 27 \text{ kg/m}^3$ (Fig. 15). These velocity cross-sections show a northward flow on Lines A, C and G during M06, and on Lines A, C, G, I and N during J07. The maximum on each cross-section shows the core of the Yucatan Current. The northward flows show maximum speeds (up to 0.8 m/s during M06 and 0.6 m/s during J07) at the northernmost lines A06 and A07, located in the Yucatan Channel, with weaker flows farther south. The Yucatan Current is not evident at Line I during M06 and Line P during J07. During M06, the northward current seen in Line A06 is about 60 km wide, with speeds up to 0.8 m/s in the 15 km wide

core. Speeds of 0.2 m/s can be observed at a depth of 200 m. Moving southward to Line C, the northward flow is divided into two main cores, one stronger current (up to 0.4 m/s) directed into the Cozumel Channel with a narrow core about 20 km wide, and the other weaker current located on the ocean side of Cozumel and reaching speeds of about 0.2 m/s. At Line G, located north of Chinchorro, the northward flow is weaker (0.2 m/s), with a core of about 10 km width, along the eastern side of the bank in the direction of the deep basin. South of Chinchorro, Line I shows a weaker northward flow, centered at 150 m depth with speeds $< 0.2 \text{ m/s}$. During J07, Line A07 included shallower stations on the Yucatan shelf than were occupied during M06. Line C shows that the core of the Yucatan Current is weaker and located farther offshore during J07 than observed during M06, where it had been stronger and closer to the coast. Lines around Chinchorro Bank during J07 show the current closer to the coast, with speeds up to 0.35 m/s at Line G, and 0.2 m/s at Line I, located south of Chinchorro. The Belizean cross-sections (Lines N and P) resemble

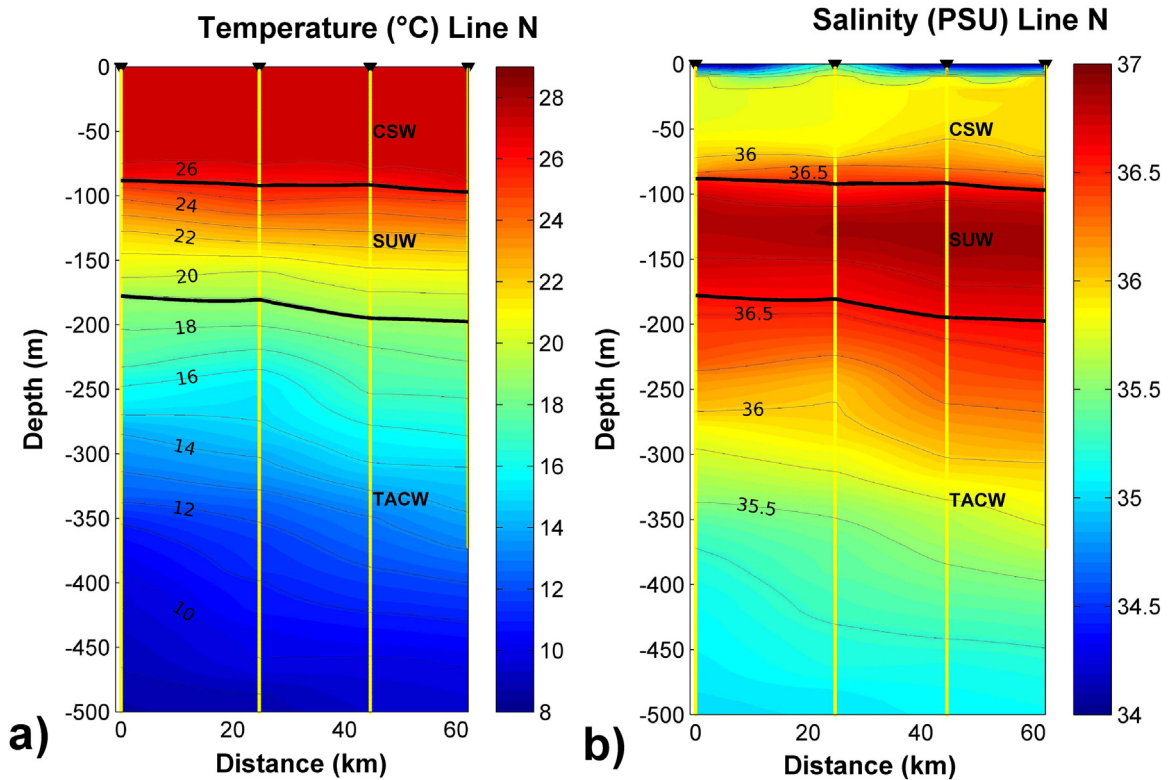


Fig. 9. Same as Fig. 5, but for the cross-section located off the Belizean coast (Line N).

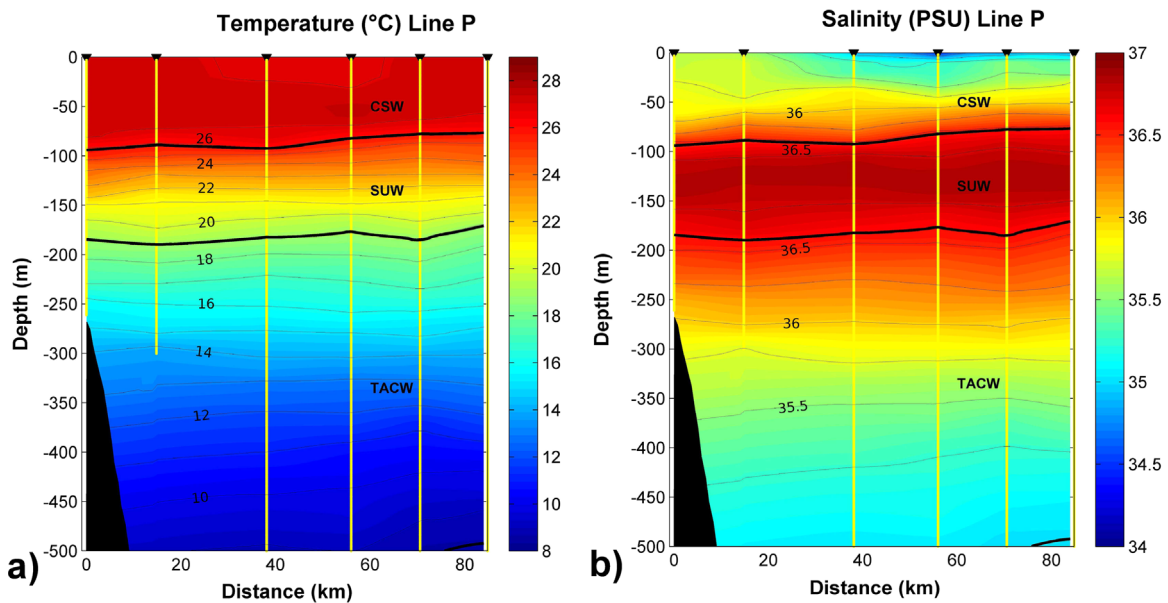


Fig. 10. Same as Fig. 5, but for the cross-section located at the southernmost section of the MBRS in the Gulf of Honduras (Line P).

Lines G and I of M06, respectively. A weak northward flow is evident at Line N, and a very weak southward flow is present at Line P.

4. Discussion

The thermohaline structure of the MBRS shows a vertical distribution that is typical of subtropical and tropical Atlantic regions, with North Atlantic Subtropical Underwater (SUW) overlying Tropical Atlantic Central Water (TACW) and flowing through the

region. Near-surface is a layer of Caribbean Surface Water (CSW), formed from the modification of SUW by land runoff and surface warming (Fig. 2). In the MBRS, this vertical structure is altered by shoaling of isolines associated with uplifting of the isopycnals where the Yucatan Current interacts with the coast, and some more localized and mild deepening of isolines in the Gulf of Honduras associated with cyclonic flow and freshwater inflows.

Based on geostrophy, the deformation of isopycnals provides information on circulation that agrees well with currents measured directly by ADCP (Carrillo et al., 2015). Although the principle of geostrophy and the coarse resolution of the station grid

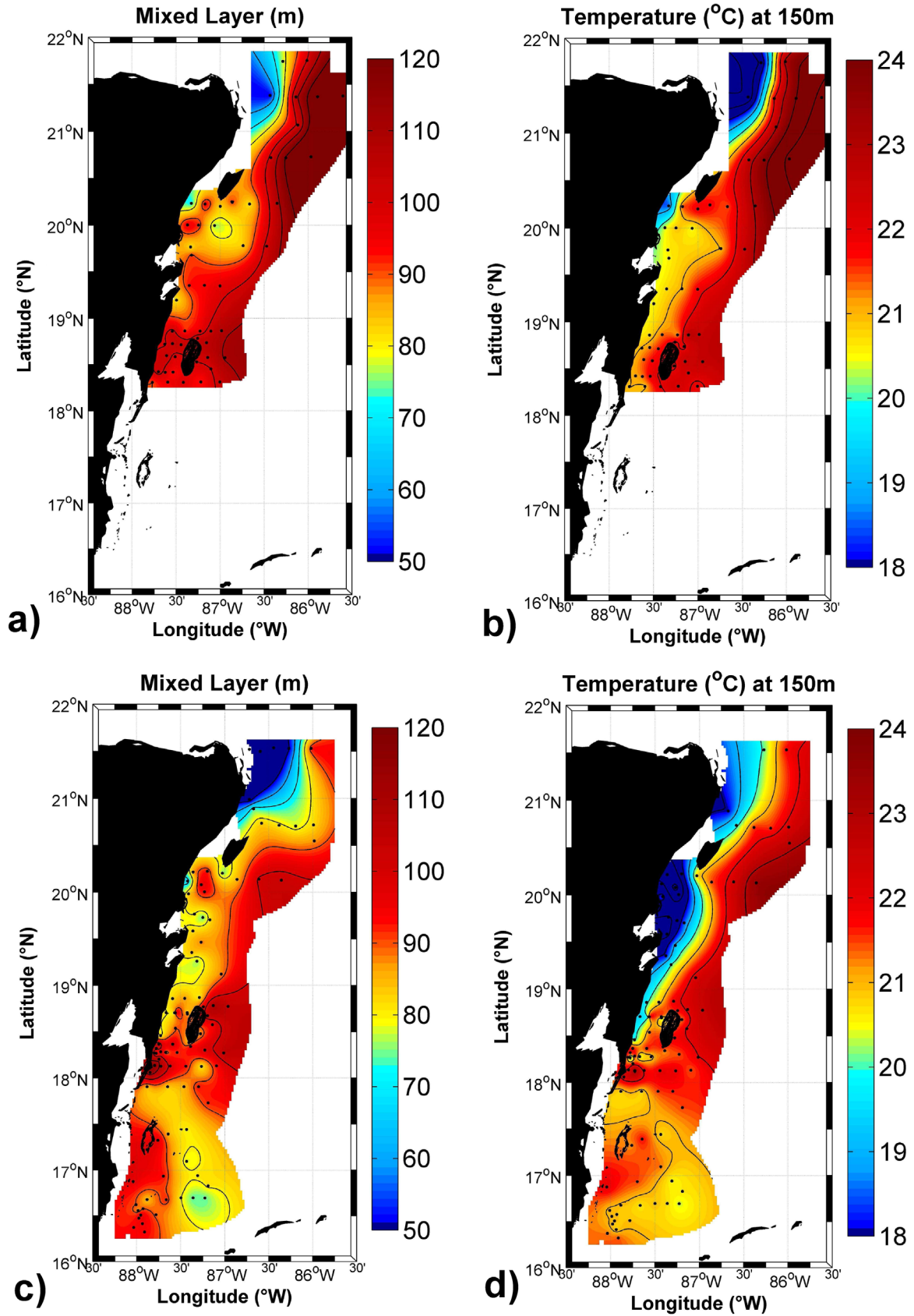


Fig. 11. a) Depth of the thermal mixed layer for M06; b) Temperature distribution at 150 m for M06; c) Depth of the thermal mixed layer for J07; and d) Temperature distribution at 150 m for J07.

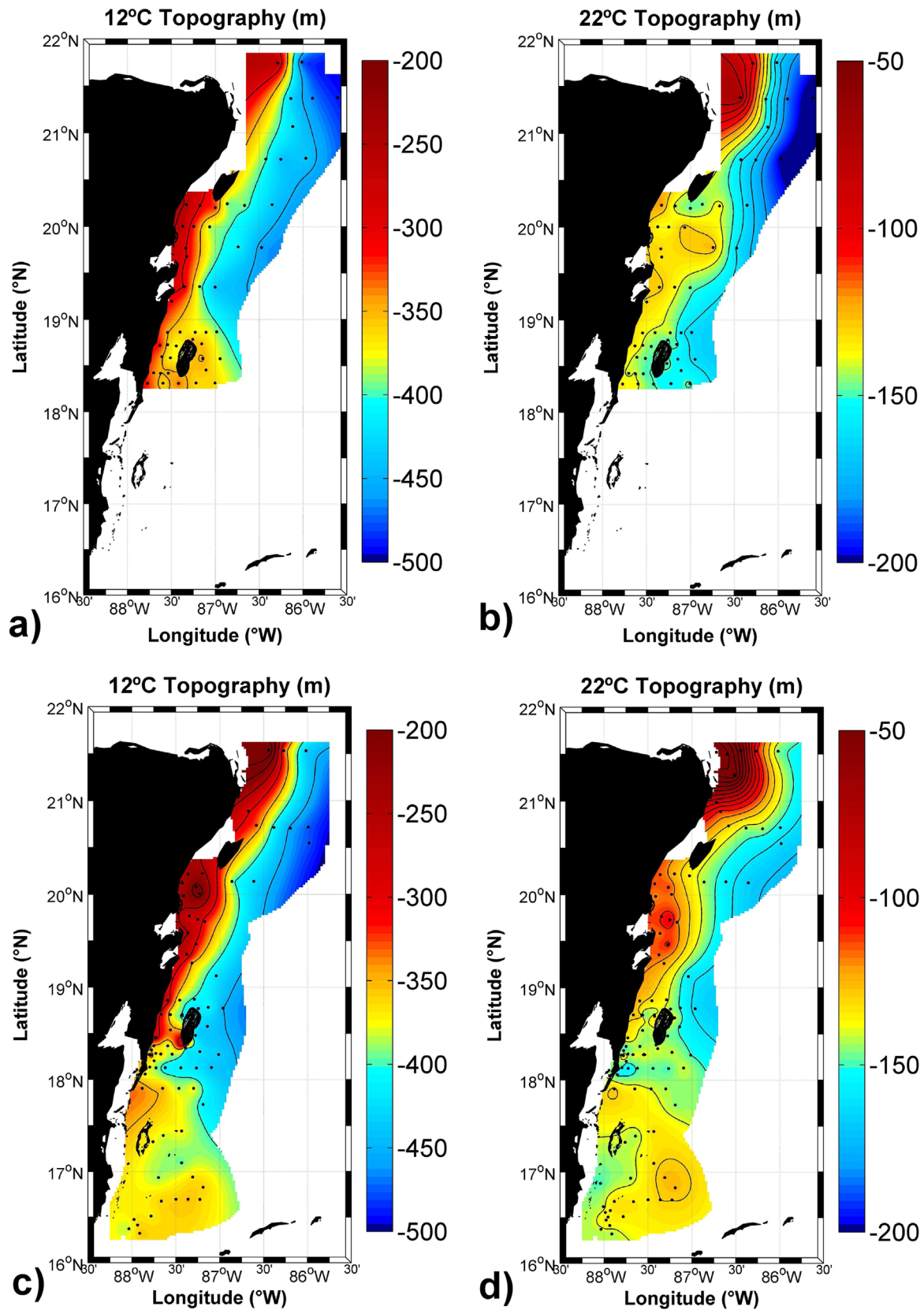


Fig. 12. a) Depth of the 12 °C isotherm for M06; b) Depth of the 22 °C isotherm for M06; c) Depth of the 12 °C isotherm for M06; and d) Depth of the 12 °C for J07.

can only resolve broad patterns (length scales of order 100 km and larger), these hydrographic data describe the primary features, including the Yucatan Current and differences between the M06 and J07 cruises and across latitudes. However, the geostrophic

fields cannot resolve submesoscale features such as the Ascension-Cozumel Coastal Eddy (Carrillo et al., 2015), the wakes behind Chinchorro Bank and Cozumel Island, or the ageostrophic flow features in the Cozumel Channel described by Chávez et al. (2003)

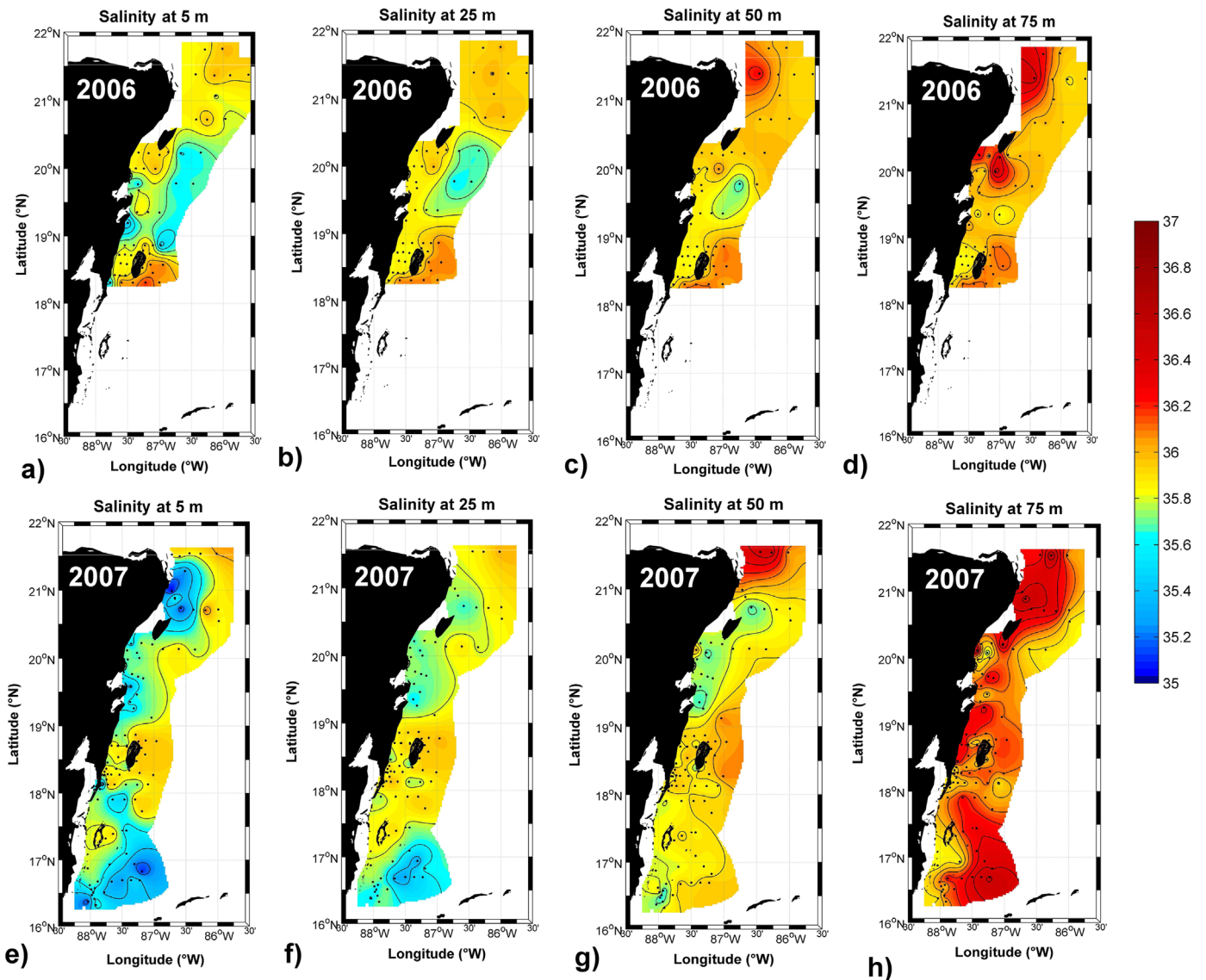


Fig. 13. Horizontal salinity distribution at a) 5 m depth during M06; b) 25 m during M06; c) 50 m during M06; d) 75 m during M06; e) 5 m depth J07; f) 25 m during J07; g) 50 m during J07; and h) 75 m during J07.

and Ochoa et al. (2005).

In the northern region, characterized by strong northward flow (Carrillo et al., 2015), coastal waters are colder and saltier in general, owing to the shoaling of temperature and salinity isolines. Described previously by Merino (1997), this current-driven upwelling raises isotherms/isohalines/isopycnals by 100 m or more. Cochran (1966; 1968) proposed that this upwelling could be induced by bottom friction associated with the strong Yucatan Current. However, Jiménez Lagunes (2004) analyzed this hypothesis using a numerical model, and the results did not support that hypothesis. Ramos Musalem (2013), by using a global circulation model (MITgcm), suggested coastally-trapped waves as the most likely forcing mechanism of the upwelling observed in this area; however, available cold water needs to be present for the vertical transport at 120 m depth. Recently, Reyes-Mendoza et al. (2016) analyzed the effect of wind and found that upwelling pulses were not correlated with wind-driven Ekman transport, suggesting that it is a process not locally controlled. We observed that an uplifting of the isotherms occurs along the MBRS while the Yucatan Current is present. In the northernmost portion of the MBRS, the uplifting of the isotherms is enhanced, allowing any vertical transport mechanism to produce the upwelling. These observations suggest

that the upwelling in the northernmost MBRS could be associated with strengthening of the Yucatan Current, and at times the SUW will outcrop at the surface near Isla Contoy, forming a marked thermal front that can be seen along the shelf edge, extending north to about 25°N latitude (Pérez de los Reyes et al., 1996). This strongest upwelling occurs where the Yucatan Current separates from the coast as the shelf widens – a phenomenon similar to that observed over the Agulhas Bank, where the Agulhas Current separates from the coast (Swart and Largier, 1987; Lutjeharms et al., 2000). This upwelling varies seasonally, weakest during autumn and winter and strongest during spring and summer (Merino, 1997) – our winter cruises were during the weaker phase of the upwelling.

Uplifting is less clear in the central MBRS, where the northward current is weaker (and absent in the southern MBRS), but it was observed as far south as Xcalak (18.25°N) during J07. Local intensification of uplifting is observed north of Bahia de la Ascension, and where the current separates from the coast forming the Ascension-Cozumel Coastal Eddy, as described in Carrillo et al. (2015).

Upwelling is important in determining water quality in the shallowest areas over the Yucatan continental shelf. This upwelled

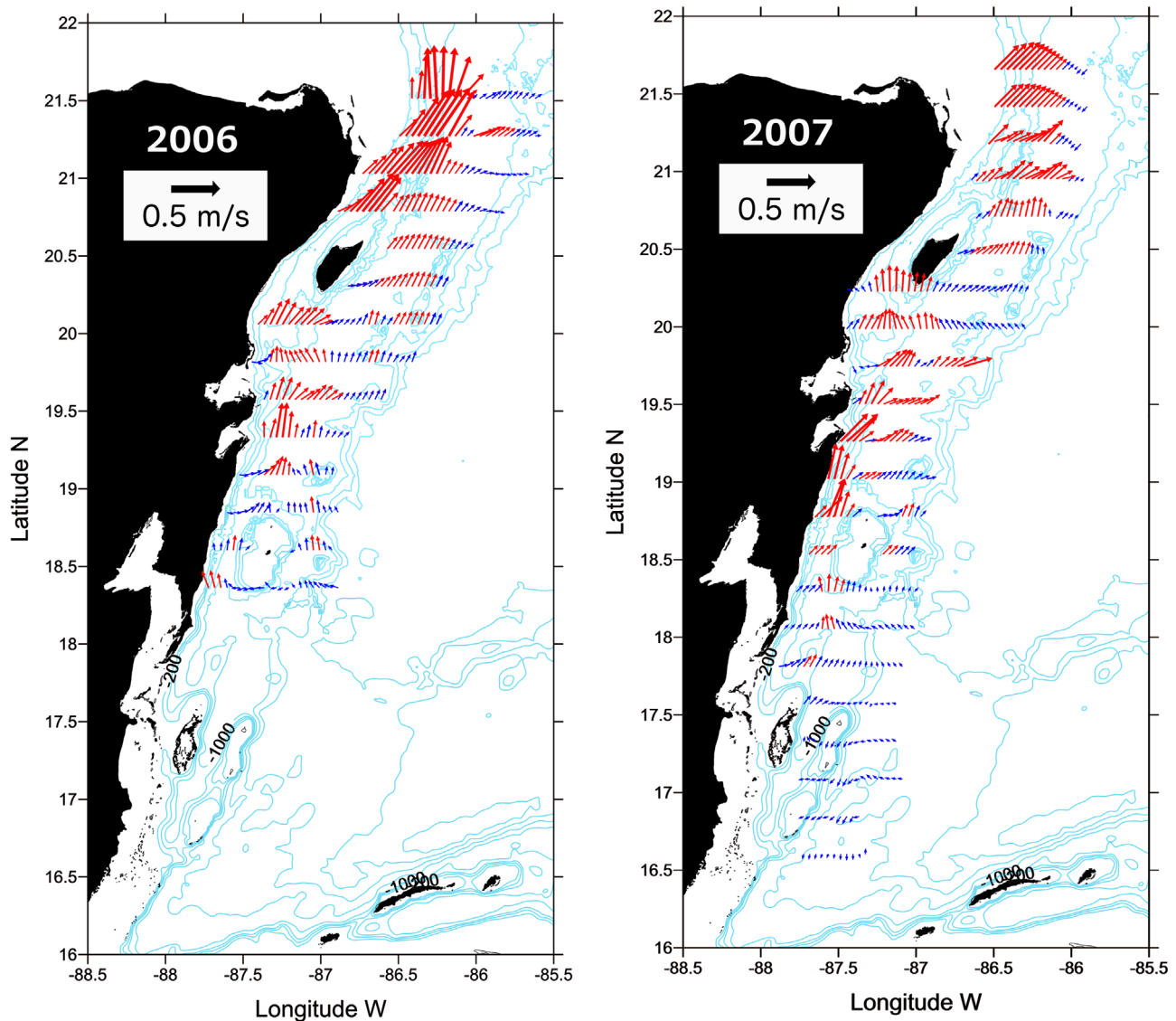


Fig. 14. Surface geostrophic velocities (in m/s) derived from hydrographic and altimetry data for a) M06; and b) J07.

water can be traced by its temperature-salinity signature (16–20 °C; 36.1–36.5), and it has been designated as Yucatan Upwelling Water (YUW) by Merino (1997), while Enriquez et al. (2013) refer to it as Caribbean Subtropical Underwater (CSUW) when observed over the Yucatan Shelf. This upwelled water also has high nutrients and low oxygen. Thus, where upwelling occurs, MBRS coastal habitats are exposed to these water properties; moreover, the upwelling enhances algal blooms, underpinning the growing concerns for harmful red tide events over the Yucatan Shelf (Enriquez et al., 2010).

Land runoff is also an important factor in coastal water quality and this is strongest in the southern MBRS where twelve rivers together discharge about $1232 \text{ m}^3 \text{ s}^{-1}$ into the Gulf of Honduras (Thattai et al., 2003), lowering salinity in the uppermost 50 m near the surface. These low-salinity waters are advected south and entrained into the Honduras Gyre (Cherubin et al., 2008), creating a regional feature (Fig. 16) and eventually being entrained in the Yucatan Current. In addition to salinity influences, land runoff may also contain biogenic materials as well as pollutants – but little is known about the loading of runoff to the Gulf of Honduras.

Low salinity waters were also observed in coastal areas farther to the north, with values about 0.6 units lower in the northern MBRS (Figs. 13 and 16) – a result which was not expected, since

there are no rivers in the Yucatan and this region is characterized by upwelling of high-salinity water. However, the Yucatan Peninsula is characterized by permeable karstic geology (Perry et al., 2002; Bauer-Gottwein et al., 2011), in which underground rivers may exist. Low salinities in coastal waters between 19°N and 20°N match up with locations where underground rivers and sinkholes are known to be connected to the sea (Smart et al., 2006; Beddows et al., 2007; Charvet, 2009). In this region, submarine groundwater discharge has been estimated at $568 \text{ m}^3 \text{ d}^{-1} \text{ m}^{-1}$ length of shoreline, but only $48 \text{ m}^3 \text{ d}^{-1} \text{ m}^{-1}$ in the northern portion near Puerto Morelos (Null et al., 2014). A single groundwater spring in the northern peninsula has been documented with a discharge of up to $34,560\text{--}40,000 \text{ m}^3 \text{ d}^{-1}$, even during the dry season (Valle-Levinson et al., 2011; Parra et al., 2015). Moreover, it has been reported that spring salinity could range between 28 and 36 modulated by changes in sea level (Valle-Levinson et al., 2011; Parra et al., 2015). Further, Enriquez et al. (2013) have previously reported low salinities on the Yucatan Shelf, north of the Peninsula. Although our observations were not close enough to the coast to trace the freshwater discharge from the karstic river system, previous studies in this area have shown significant cross-shore salinity gradients along 60 km of the coastline in the northern MBRS (Carrillo Bibriezca et al., 2008). Nevertheless, we

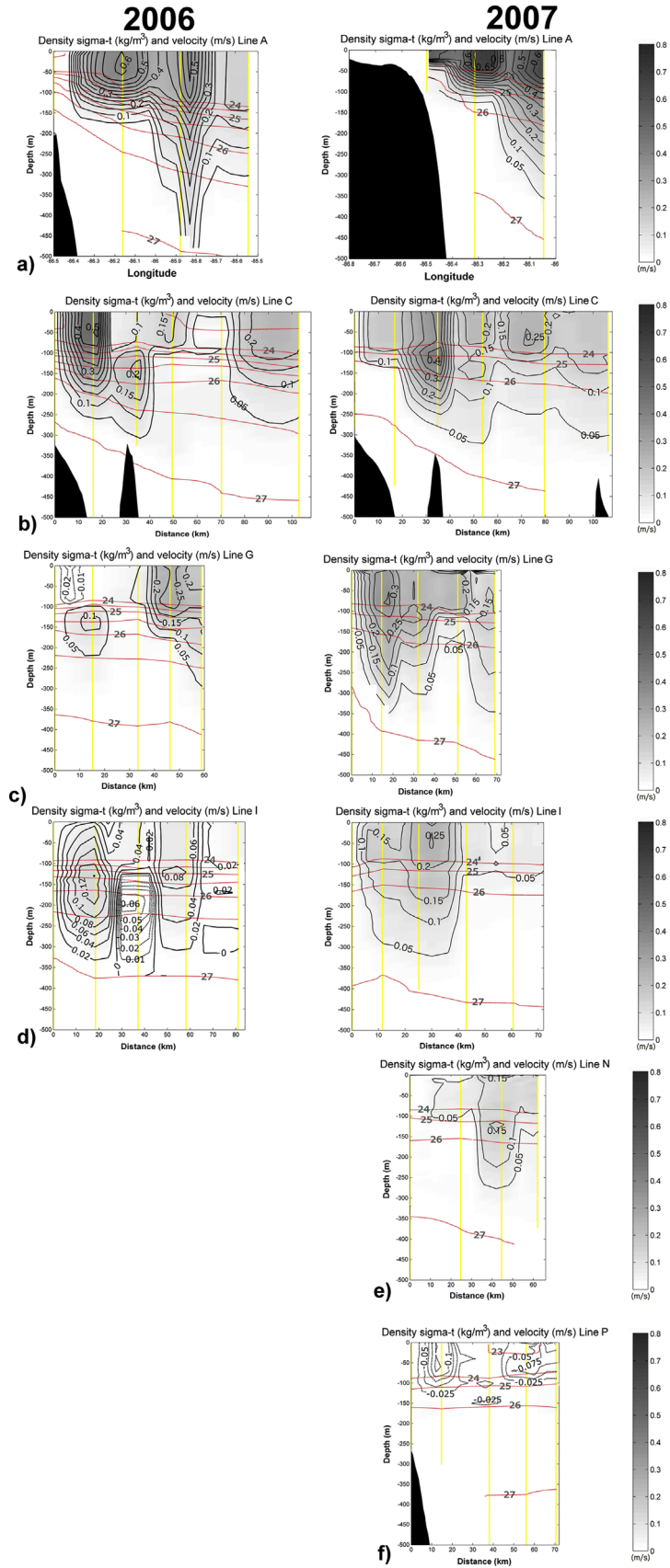


Fig. 15. Cross-sectional structure of geostrophic flow velocity (m/s) and density (kg/m^3) for M06 and J07. a) Lines A06 and A07; b) Line C; c) Line G; d) Line I; e) Line N; and f) Line P. Yellow lines represent station positions. Isopycnals are represented by red lines. Black contours and shading represent the derived geostrophic velocity perpendicular to the transect. (For interpretation of the references to color in this figure legend, the reader is referred to the web version of this article.)

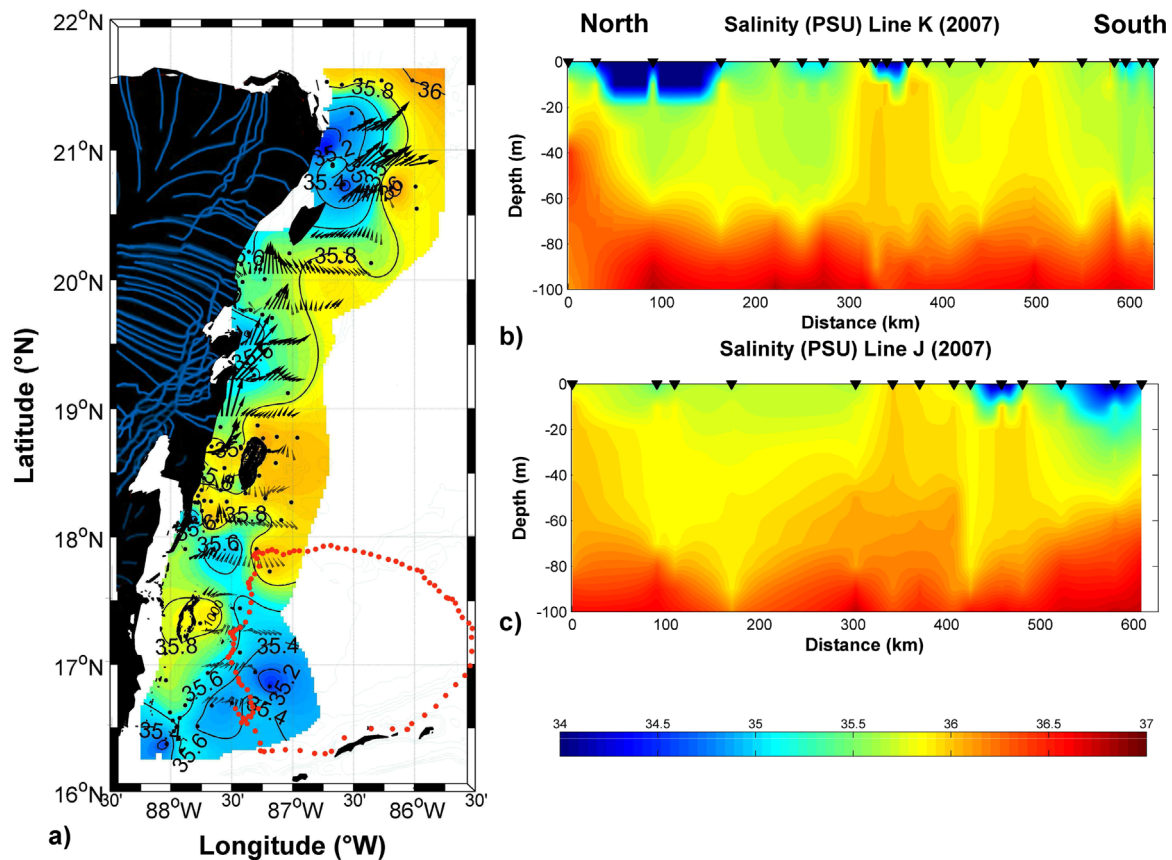


Fig. 16. a) Surface salinity for J07, with geostrophic velocity field derived from hydrographic data, and the trajectory of a surface drifter released in the Gulf of Honduras. The size, location, and shape of the Honduras Gyre were delineated by the drifter trajectory. The underground river system in the northern Yucatan Peninsula from [Bauer-Gottwein et al. \(2011\)](#) is shown in blue. b) Salinity in the uppermost 100 m on Line K, an alongshore transect 20–40 km offshore; and c) salinity in the uppermost 100 m on Line J, an alongshore transect 80–100 km offshore. (For interpretation of the references to color in this figure legend, the reader is referred to the web version of this article.)

can make an estimate of $657 \text{ m}^3 \text{ s}^{-1}$ freshwater discharge in the Ascension area by assuming a discharge of $568 \text{ m}^3 \text{ d}^{-1} \text{ m}^{-1}$ over 100 km of shoreline. From a simple salt balance, we obtain a similar order-of-magnitude estimate in J07 by noting that the coastal portion of the Yucatan Current exhibits a salinity decrease of > 0.2 over $> 25 \text{ m}$ depth and extending $> 10 \text{ km}$ offshore. Thus, it appears that land runoff (and CSW production) is equally strong in the northern MBRS, although the salinity signal is less marked probably due to the rapid flushing of coastal waters by the Yucatan Current, which means that the submarine groundwater discharge is strong.

The oceanography of the MBRS exhibits strong north-south differences, with the northern region being characterized by strong advection, upwelling and submarine groundwater discharge, while the southern region is characterized by weak currents, retention and surface discharge of land runoff. This represents marked differences in connectivity ([Muhling et al., 2013](#); [Carrillo et al., 2015](#)) and pelagic habitat ([Muhling et al., 2013](#); this paper), which can be expected to have first-order effects on the productivity and diversity of reef communities as well as their susceptibility to environmental change, including ocean warming, ocean acidification and pollutant loading. There is growing evidence that submarine groundwater discharge over the coast could lead to ocean acidification with impacts on coral reefs – and specifically in the northern MBRS ([Crook et al., 2012](#); [Crook, 2015](#)). Implications of the latitude of impingement of the Cayman Current have been mentioned previously by [Badan et al. \(2005\)](#), [Ezer et al. \(2005\)](#), and [Cherubin et al. \(2008\)](#), but little attention was given to the implications of this for coastal oceanography and the associated definition of coastal pelagic habitat, which is a primary

determinant of the state of the MBRS coral reef communities. Following the discussion of circulation in [Carrillo et al. \(2015\)](#), the mesoscale variability associated with the latitude of impingement of the Cayman Current defines a transitional region that shifts north and south over time and separates the northern and southern regions in the MBRS, yielding a northern region dynamically dominated by the Yucatan Current and a southern MBRS with lower speeds and the presence of the Honduras Gyre. This was also observed in both the geostrophic and hydrographic fields described herein. A secondary factor is the shift to karstic geology and submarine groundwater discharge in the Yucatan Peninsula. Moreover, from geostrophic calculations there were clear differences between M06 and J07 in the closeness to the coast of the Yucatan Current along its northward path as was also reported from ADCP observations ([Carrillo et al., 2015](#)). This indicates a clear meandering of the Yucatan Current probably due to the passage of mesoscale eddies.

5. Conclusions

Hydrographic data from two oceanographic cruises conducted during March 2006 and January/February 2007 provided descriptions of the thermohaline structure that are consistent with and go beyond the transport patterns outlined in [Carrillo et al. \(2015\)](#). Also, the description of water types and associated distribution of water properties are key factors in the spatial distribution of habitat along the MBRS.

The thermohaline structure in the upper 500 m of the water column along the MBRS shows a typical vertical structure for

tropical Atlantic regions represented by the three primary water masses previously defined for the Caribbean: Caribbean Surface Water (CSW), the Subtropical Underwater (SUW), and the Tropical Atlantic Central Water (TACW). The surface layer, delimited by a strong pycnocline, represents the CSW, warm with moderate salinity and oxygen levels. Underneath the CSW is the salinity maximum (36.92), representing the North Atlantic SUW with a lower oxygen concentration of 3.37–4.06 ml/L. The maximum salinity is centered at 134 ± 17 m depth during both M06 and J07 in the MBRS.

The thermohaline structure is modified by the circulation along the Mesoamerican Barrier Reef System (MBRS) and coastal freshwater interactions. The thickness and deepening or shoaling of the thermocline is a reflection of the regional dynamics and land runoff. Geostrophically-derived fields provide a reliable first approximation to the directly-measured velocity fields as they are qualitatively consistent with the ADCP observations and drifter trajectories.

Observed hydrographic fields add evidence to the regional division of the MBRS according to the latitude of impingement of the Cayman Current, since the strong flow in the Yucatan Current generates an uplifting of the isopycnals along the coast. The strongest uplifting of the water masses is observed at the northern tip of the MBRS, where the intensification of the Yucatan Current occurs in the Yucatan Channel and the widening of the Yucatan shelf can be observed. However, the uplifting of the isotherms occurs predominantly along the coast while the Yucatan Current is present. Outside of this region, the vertical structure is more related to the Caribbean deep waters with deeper values of the thermal mixed layer (100 m). In the southern part of the MBRS, weak velocities and southward flows are observed with a dominance of the Honduras Gyre.

Acknowledgments

CTD data were provided to NOAA's Coral Reef Conservation Program and are on file at the National Oceanographic Data Center (NODC) and Southeast Fisheries Science Center (SEFSC) Library. This work has been partially supported by NOAA's Coral Reef Conservation Program #1244. This work was partially supported by the base funding of NOAA's Atlantic Oceanographic and Meteorological Laboratory and Southeast Fisheries Science Center. Partial support for L. Carrillo was provided by ECOSUR. Ship time was provided by NOAA under the projects Larval Fish and Physical Oceanography Survey of the Mesoamerican Reef System, and Mesoamerican System Transport and Ecology Research. We thank the Captain and crew of the NOAA Ship *Gordon Gunter*, M. Yescas for his valuable assistance on graphics, and E. Malca and L. Vásquez-Yeomans for coordinating and for participating in the surveys. M. Lavín and Alberto Amador gave valuable advice which improved an earlier version of this manuscript, as did the comments and suggestions of the anonymous reviewers.

References

- Badan, A., Candela, J., Sheinbaum, J., Ochoa, J., 2005. Upper-layer circulation in the approaches to Yucatan Channel. In: *Circulation in the Gulf of Mexico: Observations and Models*, Geophysical Monograph Series, volume 161, AGU, pp. 57–69.
- Bauer-Gottwein, P., Gondwe, B., Charvet, G., Marín, L.E., Rebolledo-Vieyra, M., Merediz-Alonso, G., 2011. Review: The Yucatán Peninsula Karst Aquifer, Mexico. *Hydrogeol. J.* 19, 507–524. <http://dx.doi.org/10.1007/s10040-010-0699-5>.
- Beddows, P., Smart, P.L., Whitaker, F., Smith, S.L., 2007. Decoupled fresh-saline groundwater circulation of a coastal carbonate aquifer: spatial patterns of temperature and specific electrical conductivity. *J. Hydrol.* 346 (1–2), 18–32. <http://dx.doi.org/10.1016/j.jhydrol.2007.08.013>.
- Carrillo, L., Lavín, M.F., Palacios-Hernández, E., 2002. Seasonal evolution of the geostrophic circulation in the northern Gulf of California. *Estuar. Coast. Shelf Sci.* 54 (2), 157–173. <http://dx.doi.org/10.1006/ecs.2001.0845>.
- Carrillo, L., Johns, E.M., Smith, R.H., Lamkin, J.T., Largier, J.L., 2015. Pathways and hydrography in the Mesoamerican Barrier Reef System. Part 1: circulation. *Cont. Shelf Res.* 109, 164–176. <http://dx.doi.org/10.1016/j.csr.2015.09.014>.
- Carrillo Bibrzezza, L.E., Ortiz Hernández, M.C., Ramírez Manguilar, A.M., Zavala Mendoza, A., Yescas Corona, M.A., González Leija, A., Marrufo, M., Medina Esquilano, R.A., Morales Soto, R., Morales Gutierrez, S., Palacios Hernández, E., Sheinbaum, J., Zavala, J., 2008. Estudio de la calidad del agua y dispersión de contaminantes en la zona costera de la Riviera Maya (Playa del Carmen, Quintana Roo). Technical Report. CONACYT-CONAGUA, pp. 121 (http://www.ocean-ecosur.com/images/ofe/publicaciones/pdf/informes/INFORME%20FINAL%20CNA-2004-C02-3_ANEXO1.pdf).
- Chávez, G., Candela, J., Ochoa, J., 2003. Subinertial flows and transports in Cozumel Channel. *J. Geophys. Res.* 108 (C2), 3037. <http://dx.doi.org/10.1029/2002JC001456>.
- Charvet, G., 2009. *Exploration, Modeling and Management of Groundwater Resources in Northern Quintana Roo, Mexico*. Technical University of Denmark, Denmark.
- Cherubin, L.M., Kuchinke, C.P., Paris, C.B., 2008. Ocean circulation and terrestrial runoff dynamics in the Mesoamerican region from spectral optimization of SeaWiFS data and a high resolution simulation. *Coral Reefs* 27, 503–519. <http://dx.doi.org/10.1007/s00338-007-0348-1>.
- Cochrane, J.D., 1966. The Yucatan Current, upwelling off northeastern Yucatan, and currents and waters of western equatorial Atlantic. *Oceanography of the Gulf of Mexico*. Progress Rep. TAMU Ref. 66-23T, pp. 14–32.
- Cochrane, J.D., 1968. Currents and waters of the eastern Gulf of Mexico and western Caribbean, of the western tropical Atlantic Ocean, and of the eastern tropical Pacific Ocean. Department of Oceanography and Meteorology, Texas A&M University Ref. 68-8T, pp. 19–28 (unpubl. rep.).
- Cochrane, J.D., 1969. Water and circulation on Campeche Bank in May. *Special Bulletin of the Japanese Society of Fisheries Oceanography* (Prof. Uda's Commemorative Papers), pp. 123–128.
- Crook, E.D., 2015. *Corals and Ocean Acidification: Insights on Reef Community Development and Coral Calcification in an Acidified Ocean* (Ph.D. Thesis). University of California, Santa Cruz, United States, p. 208 <http://escholarship.org/uc/item/14f305xb>.
- Crook, E.D., Potts, D., Rebolledo-Vieyra, M., Hernández, L., Paytan, A., 2012. Calcifying coral abundance near low-pH springs: implications for future ocean acidification. *Coral Reefs* 31, 239–245.
- de Boyer, Montégut, Mignot, C.J., Lazar, A., Cravatte, S., 2007. Control of salinity on the mixed layer depth in the world ocean: 1. General description. *J. Geophys. Res.* 112, C06011. <http://dx.doi.org/10.1029/2006JC003953>.
- Enriquez, C., Mariño-Tapia, I., Herrera-Silveira, J., 2010. Dispersion in the Yucatan Coastal Zone: Implications for Red Tide events. *Cont. Shelf Res.* 30, 127–137. <http://dx.doi.org/10.1016/j.csr.2009.10.005>.
- Enriquez, C., Mariño-Tapia, I., Jeronimo, G., Capurro-Filigrasso, L., 2013. Thermohaline processes in a Tropical Coastal Zone. *Cont. Shelf Res.* 69, 101–109. <http://dx.doi.org/10.1016/j.csr.2013.08.018>.
- Ezer, T., Thattai, D.V., Kjerfve, B., Heyman, W.D., 2005. On the variability of the flow along the Meso-American Barrier Reef System: a numerical model study of the influence of the Caribbean current and eddies. *Ocean Dyn.* 55 (5–6), 458–475. <http://dx.doi.org/10.1007/s10236-005-0033-2>.
- Gallegos, A., 1996. *Descriptive physical oceanography of the Caribbean Sea*. Small Islands: Marine Science and Sustainable Development Coastal and Estuarine Studies 51. American Geophysical Union, United States, pp. 36–55.
- Gallegos, A., Czitrom, S., 1997. Aspectos de la oceanografía física regional del Mar Caribe. In: Lavín, M.F. (Ed.), *Oceanografía Física En México*, Monografía 3. Unión Geofísica Mexicana (UGM), México, D.F., pp. 1401–1414.
- Hernandez-Guerra, A., Joyce, T.M., 2000. Water masses and circulation in the surface layers of the Caribbean at 66°W. *Geophys. Res. Lett.* 27 (21), 3497–3500.
- Jackson, J.B.C., Donovan, M.K., Cramer, K.L., Lam, V.V., 2014. Status and trends of Caribbean Coral Reefs: 1970–2012. *Global Coral Reef Monitoring Network*. IUCN, Gland, Switzerland.
- Jaimes, B., Shay, L.K., 2009. Mixed layer cooling in mesoscale oceanic eddies during Hurricanes Katrina and Rita. *Mon. Weather Rev.* 137, 4188–4207. <http://dx.doi.org/10.1175/2009MWR2849.1>.
- Jiménez Lagunes, L., 2004. *Modelación Numérica del Afloramiento en la Plataforma Continental de Yucatán*. CICESE, México.
- Kara, A.B., Rochford, P.A., Hurlburt, H.E., 2003. Mixed layer depth variability over the global ocean. *J. Geophys. Res.* 108 (C3), 3079. <http://dx.doi.org/10.1029/2000JC000736>.
- Lutjeharms, J.R.E., Cooper, J., Roberts, M., 2000. Upwelling at the inshore edge of the Agulhas Current. *Cont. Shelf Res.* 20, 737–761.
- Lambert, R.B., Sturges, W., 1977. A thermohaline staircase and vertical mixing in the thermocline. *Deep-Sea Res.* 24, 211–222.
- Merino, M., 1997. Upwelling on the Yucatan shelf: hydrographic evidence. *J. Mar. Syst.* 13, 101–121.
- Morrison, J.M., Nowlin, W.D., 1982. General distribution of water masses within the eastern Caribbean Sea during the winter of 1972 and fall of 1973. *J. Geophys. Res.* 87 (C6), 4207–4229.
- Muhling, B.A., Smith, R.H., Vasques-Yeomans, L., Lamkin, J.T., Johns, E.M., Carrillo, L., Sosa-Cordero, E., Malca, E., 2013. Larval reef fish assemblages and mesoscale oceanographic structure along the Mesoamerican Barrier Reef System. *Fish. Oceanogr.* 22 (5), 409–428.

- Nichols, C.R., Williams, R.G., 2009. *Encyclopedia of Marine Science. Facts on File, USA*, p. 626.
- Null, K.A., Kneee, K.L., Crook, E.D., de Sieyes, N.R., Rebolledo-Vieyra, M., Hernández-Terrones, L., Paytan, A., 2014. Composition and fluxes of submarine groundwater along the Caribbean coast of the Yucatan Peninsula. *Cont. Shelf Res.* 77, 38–50. <http://dx.doi.org/10.1016/j.csr.2014.01.011>.
- Ochoa, J., Candela, J., Badan, A., Sheinbaum, J., 2005. Ageostrophic fluctuations in Cozumel Channel. *J. Geophys. Res.* 110 (C2), C02004. <http://dx.doi.org/10.1029/2004JC002408>.
- Parra, S.M., Valle-Levinson, A., Marino-Tapia, I., Enriquez, C., 2015. Salt intrusion at a submarine spring in a fringing reef lagoon. *J. Geophys. Res. Ocean.* 120, 2736–2750. <http://dx.doi.org/10.1002/2014JC010459>.
- Pérez de los Reyes, R., Victoria del Río, I., Signoret Poillon, M., Gallegos García, A., Penié Rodríguez, I., Gil Varona, C., Bulit, C., Melo González, N., Müller-Karger, F., Cerdeira Estrada, S., Merino Ibarra, M., 1996. REPORTE De UN frente hidrologico Al NE De La Peninsula De Yucatan. *Boletín De La Sociedad Meteorologica De Cuba*. 2(1), ISSN-1025-921X. Available at: (<http://cake.fiu.edu/Melo/REPORTE%20DE%20UN%20FRENTE%20HIDROLOGICO%20AL%20NE%20DE%20LA%20PENINSULA%20DE%20YUCATAN.pdf>).
- Perry, E., Velázquez-Oliman, G., Marin, L., 2002. The hydrogeochemistry of the Karst Aquifer System of the northern Yucatan Peninsula, Mexico. *Int. Geol. Rev.* 44, 191–221.
- Ramos Musalem, A.K., 2013. *Estudio numérico de los forzamientos que generan la surgencia de Yucatán (Bsc. Thesis)*. UNAM, Mexico, p. 77.
- Reyes-Mendoza, O., Mariño-Tapia, I., Herrera-Silveira, J., Ruiz-Martínez, G., Enriquez, C., Largier, J.L., 2016. The effects of wind on upwelling off Cabo Catoche. *J. Coast. Res.* . <http://dx.doi.org/10.2112/JCOASTRES-d-15-00043.1> (in press)
- Rio, M.H., Hernandez, F., 2004. A mean dynamic topography computed over the world ocean from altimetry, in situ measurements, and a geoid model. *J. Geophys. Res.* 109, C12032. <http://dx.doi.org/10.1029/2003JC002226>.
- Ruiz, E.G., 1979. *Upwelling North of the Yucatan Peninsula (M.Sc. Dissertation)*. Texas A&M University Department of Oceanography, College Station, TX, p. 85.
- Smart, P.L., Beddows, P.A., Doerr, S., Smith, S.L., Whitaker, F.F., 2006. Cave development on the Caribbean coast of the Yucatan Peninsula, Quintana Roo, Mexico, Geological Society of America Special Paper 404, Perspectives on Karst Geomorphology, Hydrology, & Geochemistry, pp. 105–128. doi: [http://dx.doi.org/10.1130/2006.2404\(10\)](http://dx.doi.org/10.1130/2006.2404(10)).
- Swart, V.P., Largier, J.L., 1987. Thermal structure of Agulhas Bank waters. In: Payne, A.I.L., Gulland, J.A., Brink, K.H. (Eds.), *The Benguela and Comparable Ecosystems*. South African Journal of Marine Science, vol. 5, pp. 243–254.
- Thattai, D., Kjerfve, B., Heyman, W.D., 2003. Hydrometeorology and variability of water discharge and sediment load in the inner Gulf of Honduras, Western Caribbean. *J. Hydrometeorol.* 4, 985–995.
- Tomczak, M., Godfrey, J.S., 2003. *Regional Oceanography: An Introduction*, 2nd edition. Daya Publishing House, Delhi, p. 390.
- Wüst, G., 1964. *Stratification and Circulation in the Antillean-Caribbean Basins*. Columbia University Press, Palisades, New York, p. 201.
- Valle-Levinson, A., Mariño-Tapia, I., Enriquez, C., Waterhouse, A.F., 2011. Tidal variability of salinity and velocity fields related to intense point-source submarine groundwater discharges into the coastal ocean. *Limnol. Oceanogr.* 56 (4), 1213–1224. <http://dx.doi.org/10.4319/lo.2011.56.4.1213>.